Energy Advances

ROYAL SOCIETY OF CHEMISTRY

PAPER

View Article Online
View Journal | View Issue

Cite this: *Energy Adv.*, 2023, 2, 1390

On the relationship of the effective mobility and photoconductance mobility in organic solar cells†

Joachim Vollbrecht, ‡*[a] Nurlan Tokmoldin, *[a] Bowen Sun,[a] Elifnaz Saglamkaya,[a] Lorena Perdigón-Toro,[a] Seyed Mehrdad Hosseini,[a] Jae Hoon Son,[b] Han Young Woo,[b] Safa Shoaee[ac] and Dieter Neher[a]

The efficiency of organic solar cells has increased significantly in the recent years due to the continued improvement in material properties, including the charge carrier mobilities within the bulk heterojunction. However, common strategies to measure the mobility of electrons and holes, such as the space-charge-limited-current approach, rely on purpose-made single carrier diodes, which are operated in the injection regime. Alternatively, impedance spectroscopy measurements can yield an effective mobility as well as a photoconductance mobility for solar cells under realistic operating conditions. There exist various theoretical interpretations that relate the experimentally determined values of the effective mobility with the mobility of the individual charge carriers (*i.e.* electrons and holes). Furthermore, the relationship between the effective and photoconductance mobility has not been clarified yet. This study shows how the effective and photoconductance mobilities can be combined in a system of equations to calculate the individual mobilities of the faster and slower carriers. Finally, these considerations are applied to determine individual carrier mobilities in several blend systems, including fullerene-based P3HT:$PC_{60}BM$ solar cells, as well as non-fullerene devices based on PM6:Y11-N4, PM6:Y5, PPDT2FBT:Y6, PM6:Y11, PM6:N4, and PM6:Y6. These results were validated with mobility values obtained *via* the space-charge-limited-current approach.

Received 21st March 2023,
Accepted 19th July 2023

DOI: 10.1039/d3ya00125c

rsc.li/energy-advances

1. Introduction

The field of organic solar cells has experienced significant improvements in recent years. Organic photovoltaics (OPV) distinguish themselves with the potential of a low priced, solution based, scalable production, and their applicability on lightweight, flexible substrates, which are unique selling points of all types of organic electronic technologies.[1–5] There is a considerable commercial potential for OPVs, if certain thresholds in device stability, power conversion efficiency (PCE $\geq$ 15%) and production cost are achieved.[6,7] One of these aforementioned thresholds has recently been exceeded in laboratory scale devices (PCE $>$ 19%),[8–13] which can mostly be attributed to the successful use of non-fullerene acceptors (NFA) that were developed through continuous efforts to replace the hitherto ubiquitous fullerene-based acceptors, such as $PC_{60}BM$.[14–24] In particular, solar cells based on the polymer donor PM6 and the NFA Y6 are representative of this recent performance increase.[25–27] Furthermore, numerous different synthetic strategies have been employed and investigated in search for viable NFAs in the past.[28–33] Organic solar cells typically have a two-component active layer in a bulk-heterojunction (BHJ) configuration, consisting of a donor and acceptor material with a large donor–acceptor (D:A) interface (*cf.* Fig. 1).[34] The need for this configuration arises due to the small dielectric constant of organic semiconductors ($\varepsilon_r \approx 3$), which leads to the formation of bound excitons.[35,36] The excitons can split into free charge carriers at the D:A interface, owing to the energy level differences. Matching these different energy levels at the D:A interface is critical for the efficient generation and extraction of free electrons and holes, which affects the overall performance of the organic solar cell. It is a common approach to treat the BHJ active layer as an effective medium, and some device characterization analyses operate on the basis of an effective charge carrier mobility μ_{eff} that replaces individual mobilities of electrons and holes.[37] The need for dedicated, single carrier diodes to determine the mobilities of the individual carriers through space-charge-limited-current (SCLC) measurements, which have to be studied at voltages that are outside of the

[a] *Institute of Physics and Astronomy, University of Potsdam, Potsdam, Germany. E-mail: vollbrecht@uni-potsdam.de, tokmoldin@uni-potsdam.de*
[b] *Department of Chemistry, Korea University, Seoul, Republic of Korea*
[c] *Paul-Drude-Institut für Festkörperelektronik, Leibniz-Institut im Forschungsverbund Berlin e.V, Berlin, Germany*

† Electronic supplementary information (ESI) available. See DOI: https://doi.org/10.1039/d3ya00125c

‡ Current address: Institut für Solarenergieforschung GmbH, Emmerthal, Germany.

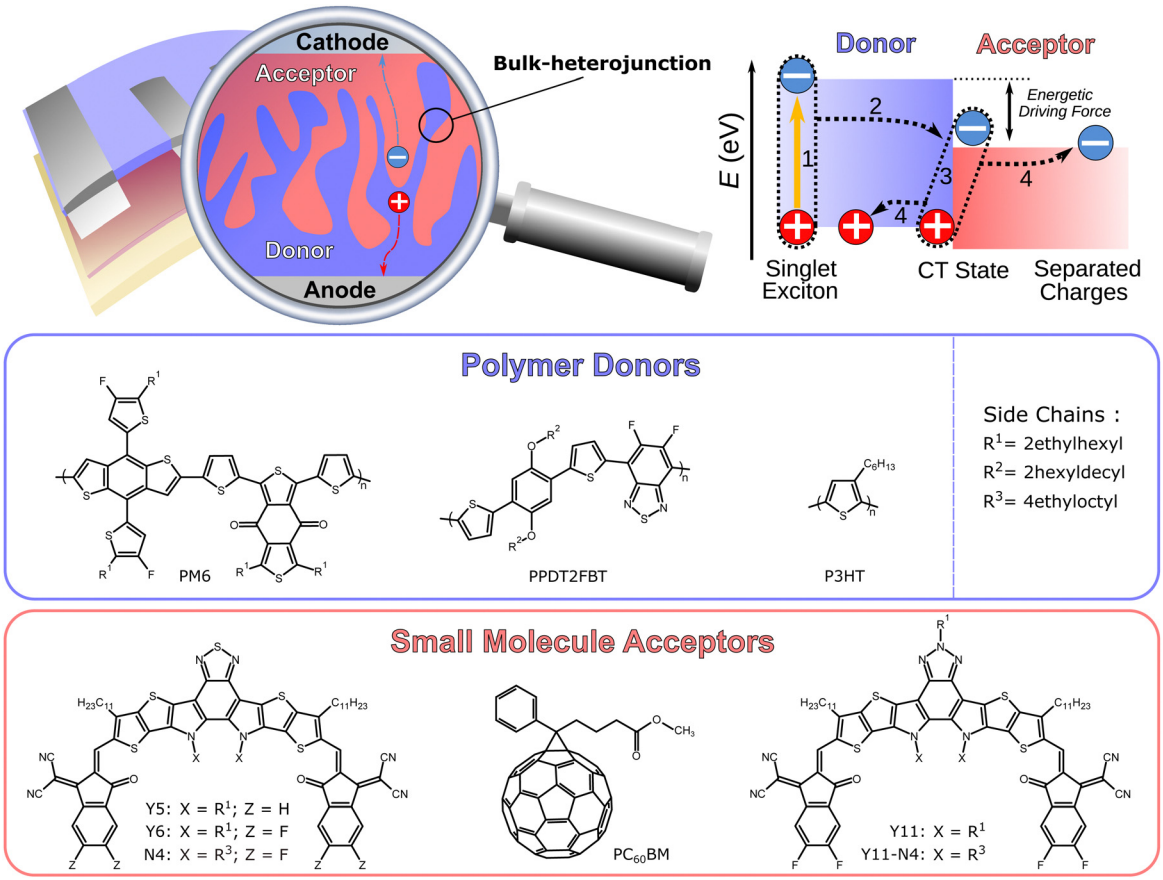

Fig. 1 Schematic depiction of an organic solar cell and its bulk-heterojunction active layer consisting of a donor polymer and acceptor small molecule. The relevant energy levels involved in the photogeneration: (1) formation of exciton *via* photon absorption; (2) exciton diffusion to the donor:acceptor (D:A) interface and charge transfer (CT) state; (3) charge separation; (4) extraction of free charge carriers to the electrodes. Chemical structures of the polymer donors PM6, PPDT2FBT, and P3HT as well as the small molecule acceptors Y5, Y6, N4, $PC_{60}BM$, Y11, and Y11-N4.

typical operating range of solar cells, can be avoided by this strategy. Moreover, the effective mobility μ_{eff} has been successfully used for the quantification of recombination and extraction dynamics.[38,39]

The experimentally attainable effective mobility μ_{eff}^{exp} of charge carriers in organic solar cells has hitherto been referred to as a mean value between the slower and faster carrier mobilities (μ_{min} and μ_{max}).[37] This study provides an overview of the various descriptions of the effective mobility and proposes a combination of experimental measurements which yield relevant mobility values, followed by the investigation of different types of blend systems over a wide range of light intensities. Devices with active layers based on P3HT:$PC_{60}BM$, PM6:Y11-N4, PM6:Y5, PPDT2FBT:Y6, PM6:Y11, PM6:N4, and PM6:Y6, the latter with varying electron transport layers and thicknesses (*cf.* Fig. 1 and Fig. S1 in the ESI†), were investigated, demonstrating the general applicability of the aforementioned approach.

2. Fundamental principles

Measuring individual carrier mobilities in complete solar cells at operating conditions poses a significant challenge, since injection/extraction and transport of both negative and positive charge carriers occur simultaneously. Let us consider the total current density in a solar cell in the presence of an electric field as the sum of the current densities resulting from the movement of electrons and holes:

$$J_{tot} = J_n + J_p = q \cdot n \cdot \mu_n \cdot E + q \cdot p \cdot \mu_p \cdot E, \quad (1)$$

where q is the elementary charge, E is the electric field within the active layer, n and p are the charge carrier densities for electrons and holes, and $\mu_{n,p}$ are the respective mobilities. Considering the relationship of the average charge carrier density $n_{av} = n = p$, which is relevant for higher light intensities when the excess carrier density significantly exceeds the dark carrier density, the following expression can be obtained:

$$J_{tot} = q \cdot E \cdot n_{av} \cdot (\mu_n + \mu_p) = 2q \cdot E \cdot n_{av} \cdot \mu_{eff}, \quad (2)$$

where the effective mobility is introduced due to the inability to distinguish between the faster and slower carrier mobilities. As suggested by eqn (2), the effective mobility encompasses the transport properties of both charge carriers; its relationship to the individual carrier mobilities remains at the focus of numerous studies. Experimentally the effective mobility can be accessed by taking into account the relationship of the current

density J, charge carrier density n_{av}, and the internal voltage V_{int} under steady-state conditions:

$$\mu_{eff}^{exp} = \frac{1}{2}\cdot\frac{J}{qn_{av}}\cdot\frac{L}{V_{int}} = \frac{1}{2}\cdot\underbrace{\frac{J}{qn_{av}}}_{=v_D}\cdot\underbrace{\frac{L}{(V_{OC}-V_{cor})}}_{=E^{-1}}, \quad (3)$$

where v_D is the charge carrier velocity, E is the electric field within the active layer, q is the elementary charge, L is the active layer thickness, V_{OC} is the open-circuit voltage, and V_{cor} is the applied voltage corrected for the series resistance R_s ($V_{cor} = V_{app} - J{\cdot}R_s$).[36,39] The current density J and the associated internal voltage V_{int} can be easily obtained *via* standard J–V-characteristics. In contrast, the determination of the charge carrier density n_{av} relies on more sophisticated measurement techniques, such as charge extraction, transient photovoltage/photocurrent, or impedance/capacitance spectroscopy.[40–46] Nevertheless, the necessary values to calculate the effective mobility according to eqn (3) can be obtained for solar cells under realistic operating conditions. Notably, determination of the effective mobility is not possible in the vicinity of the open-circuit voltage due to the denominator in eqn (3) approaching zero. Under the assumption of the equality between the excess electron and hole densities, as well as in absence of strong doping and dark charge injection, the sum of the electron and hole mobilities at the open-circuit condition can be obtained from the device quasi-steady-state photoconductivity σ_{ph}.[47] Specifically, the relationship between the photoconductance G_{ph} and the charge carrier density n gives:

$$\mu_{ph} = \mu_n + \mu_p = \frac{\sigma_{ph}}{qn} = \frac{L\cdot G_{ph}}{q\cdot A\cdot n}, \quad (4)$$

where μ_{ph} is the photoconductance mobility, q is the elementary charge, A is the active area, and L is the active layer thickness. Furthermore, with $G_{ph} = \frac{\partial I}{\partial V}$, we obtain:

$$\mu_{ph} = \frac{L}{q\cdot A\cdot n}\frac{\partial I}{\partial V} = \frac{L}{q\cdot n}\frac{\partial J}{\partial V}, \quad (5)$$

which, upon comparison with eqn (3), results in the equivalence:

$$\mu_{ph} = 2\mu_{eff}^{exp}, \quad (6)$$

under the condition that $\partial J/\partial V = J/V_{int}$ and $\mu_n = \mu_p$. Thus, eqn (6) relies on the approximation of the J–V-curve at $V = V_{int}$ (or $V = V_{OC}$); the relationship is not applicable beyond these voltages. Nonetheless, eqn (6) is important, since the effective mobility μ_{eff}^{exp} is not defined at V_{OC}, as can be seen by the numerator ($J = 0$) and the denominator ($V_{int} = 0$) in eqn (3). Therefore, in previous studies μ_{eff}^{exp} (V_{OC}) was obtained *via* linear interpolation or extrapolation of the experimentally determined values of μ_{eff}^{exp} at voltages close to open-circuit, or was left undetermined under these conditions.[36,39]

The relationship between the effective mobility and independently measured carrier mobilities has been previously rationalised in terms of the encounter limited and morphology dependent recombination models, which represent the bimolecular carrier recombination coefficient k as a function of mobility.[48] As such, depending on the size of the domains within a bulk heterojunction, k has been found to correlate with an arithmetic, harmonic, or geometric mean of the individual carrier mobilities. For the detailed description of this topic we refer the reader to more dedicated review articles.[37,48] In the framework of this paper, we focus on the various definitions of the effective mobility in terms of the respective means of the electron and hole mobilities.

One fundamental interpretation of the effective mobility relies on the harmonic mean of μ_n and μ_p:

$$\mu_{eff}^{har} = \frac{2\mu_n\mu_p}{\mu_n + \mu_p}. \quad (7)$$

Here, it is assumed that under steady state conditions the flux of electrons leaving the device must be the same as the flux of holes.[49] Importantly, the combination of the definition of the effective mobility *via* the harmonic mean μ_{eff}^{har} and the photoconductance mobility μ_{ph} depicted above (*cf.* eqn (4)) allows determining the individual mobilities of the two types of charge carriers. This is possible, since there are now two unknown variables, namely μ_n and μ_p, and two equations. Instead of μ_n and μ_p, the variables μ_{max} and μ_{min} are chosen, since the suggested method does not allow to identify the type of charge carrier. The solution of the proposed system of equations yields:

$$\mu_{max}^{har} = \frac{1}{2}\left[\mu_{ph} + \sqrt{\mu_{ph}\left(\mu_{ph} - 2\mu_{eff}^{har}\right)}\right], \quad (8)$$

$$\mu_{min}^{har} = \frac{1}{2}\left[\mu_{ph} - \sqrt{\mu_{ph}\left(\mu_{ph} - 2\mu_{eff}^{har}\right)}\right]. \quad (9)$$

Hence, if the proposed relationship between the effective mobility μ_{eff}^{har} and the photoconductance mobility μ_{ph} is reliable, it should be possible, according to eqn (8) and (9), to calculate the maximum and minimum mobility (μ_{max}^{har} and μ_{min}^{har}) for an appropriately tested solar cell.

Another interpretation of the effective mobility in relation to the individual mobilities of the two types of charge carriers is based on their geometric mean:[50–52]

$$\mu_{eff}^{geo} = \sqrt{\mu_n\cdot\mu_p}. \quad (10)$$

In this case, the solutions to the system of equations to determine the maximum and minimum mobilities have to be adjusted accordingly. Thus, the respective expressions for individual mobilities change as follows:

$$\mu_{max}^{geo} = \frac{1}{2}\left[\mu_{ph} + \sqrt{{\mu_{ph}}^2 - 4\mu_{eff}^{geo2}}\right], \quad (11)$$

$$\mu_{min}^{geo} = \frac{1}{2}\left[\mu_{ph} - \sqrt{{\mu_{ph}}^2 - 4\mu_{eff}^{geo2}}\right]. \quad (12)$$

There also exist empirical estimates for the effective mobility, which put a more significant weight on the smaller carrier mobility:[53]

$$\mu_{eff}^{emp} = \sqrt{{\mu_{max}}^{0.4}\cdot{\mu_{min}}^{1.6}}. \quad (13)$$

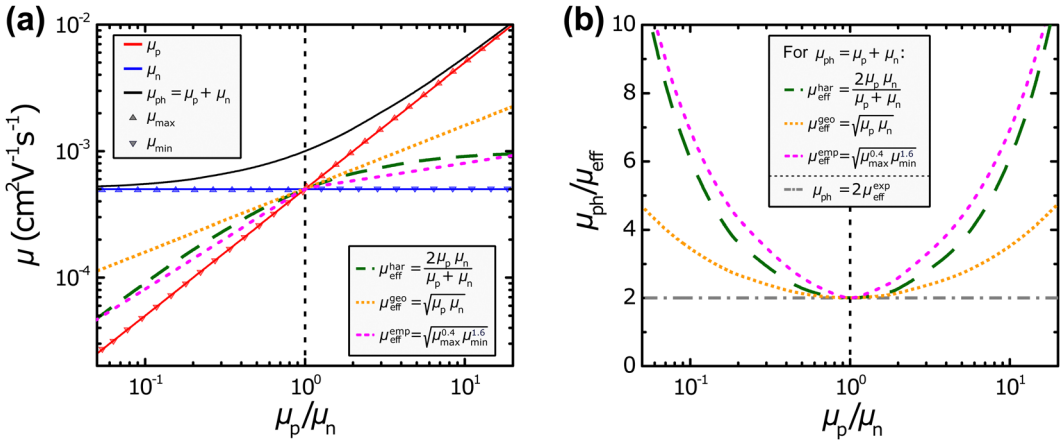

Fig. 2 (a) Different definitions of the effective mobility μ_{eff} and photoconductance mobility μ_{ph} as well as (b) the resulting ratio μ_{ph}/μ_{eff} in relation to the ratio of the hole and electron mobility μ_p/μ_n.

The different interpretations of the photoconductance and effective mobility in relationship to the different ratios of μ_p/μ_n are depicted in Fig. 2. In the plots shown in Fig. 2(a), different values for μ_p and μ_n have been used to calculate μ_{ph}, μ_{eff}^{har}, μ_{eff}^{geo}, and μ_{eff}^{emp}, respectively. However, it should be noted that space-charge effects that can have an influence particularly once significantly imbalanced mobilities are present, have not been considered in these examples.

One of the obvious aspects that is shared by all the aforementioned definitions of the effective mobility is that they are all equal to the value of the individual mobilities in the presence of balanced charge transport ($\mu_{eff} = \mu_p = \mu_n$). This also highlights the need for the factor "2" for the harmonic case, because otherwise the harmonic effective mobility μ_{eff}^{har} would converge to half of the individual mobilities.[49] Furthermore, the effective mobilities all follow, to a varying extent, the smaller individual mobility μ_{min}, as should be expected from the equations listed above. In particular, the harmonic and empirical effective mobilities (μ_{eff}^{har} and μ_{eff}^{emp}) exhibit rather similar values throughout the different mobility ratios μ_p/μ_n. In contrast, the geometric effective mobility μ_{eff}^{geo} shows more pronounced deviations to the other two types of definitions of the effective mobility, specifically at more imbalanced ratios of μ_p/μ_n. Under such conditions, the geometric effective mobility μ_{eff}^{geo} yields values that are noticeably larger than the minimum mobility μ_{min}. In Fig. 2(b), the ratios between the photoconductance mobility μ_{ph} as described in eqn (4) and the various definitions of the effective mobility (*i.e.* μ_{eff}^{har}, μ_{eff}^{geo}, μ_{eff}^{emp}; *cf.* eqn (7), (10) and (13), respectively) are visualized at different mobility ratios μ_p/μ_n. The case of a linear relationship between the photoconductance and effective mobility ($\mu_{ph} = 2\mu_{eff}^{exp}$, *cf.* eqn (6)) has also been included in form of the horizontal, dash-dotted line. This visualization also depicts the convergence of all the different definitions for the balanced mobilities ($\mu_p/\mu_n = 1$). In addition, Fig. 2(b) shows the necessary ratios of μ_{ph}/μ_{eff} to obtain μ_{min} and μ_{max} *via* the relationships derived in eqn (8) and (9) for the harmonic definition as well as the relationships derived in eqn (11) and (12) for the geometric definition of the effective mobility. No results can be expected for the individual mobilities, if the ratio $\mu_{ph}/\mu_{eff} < 2$, regardless of what exact definition is chosen for the effective mobility. As we will see later, there are several experimental examples, for which $\mu_{ph}/\mu_{eff} < 2$ is the case, leading to undefined μ_{min} and μ_{max}.

3. Results and discussion

In this study, nine different organic solar cells were investigated over a wide range of light intensities to test the hypothesis presented above in Section 2. Namely, solar cells based on P3HT:PC$_{60}$BM, PM6:Y11-N4, PM6:Y5, PPDT2FBT:Y6, PM6:Y11, PM6:N4, and PM6:Y6, the latter with varying electron transport layers and thicknesses, were fabricated (*cf.* Fig. 1). The photovoltaic parameters of the tested devices, including the open-circuit voltage V_{OC}, the short-circuit current density J_{SC}, the fill factor FF, and power conversion efficiency PCE under 1 sun illumination as well as the BHJ thickness L, are listed in Table 1. The effective mobilities at varying light intensities and applied biases were obtained from the measured J–V-characteristics and charge carrier densities using eqn (3). The latter were determined, as described in more detail in the ESI,† *via* the capacitance spectra extracted from the impedance measurements (*cf.* Section S13 and S23 in the ESI†).[45,46]

Table 1 Photovoltaic parameters obtained from the J–V-characteristics and active layer thickness of the studied solar cells in order of their PCE

Solar cell	V_{OC} (mV)	J_{SC} (A m^{-2})	FF	PCE (%)	L (nm)
P3HT:PC$_{60}$BM	725.0	72.3	0.6245	3.27	90
PM6:Y11-N4	835.5	155.0	0.6179	8.00	80
PM6:Y5	973.5	164.0	0.5301	8.46	100
PPDT2FBT:Y6	685.7	263.4	0.5763	10.41	80
PM6:Y11	863.1	250.7	0.5253	11.37	90
PM6:N4	779.5	234.2	0.6550	11.96	110
PM6:Y6 (PDINO)	815.3	258.4	0.6788	14.30	100
PM6:Y6 (PDINO)	825.5	272.0	0.6476	14.54	90
PM6:Y6 (PDINN)	815.9	270.9	0.7044	15.57	100

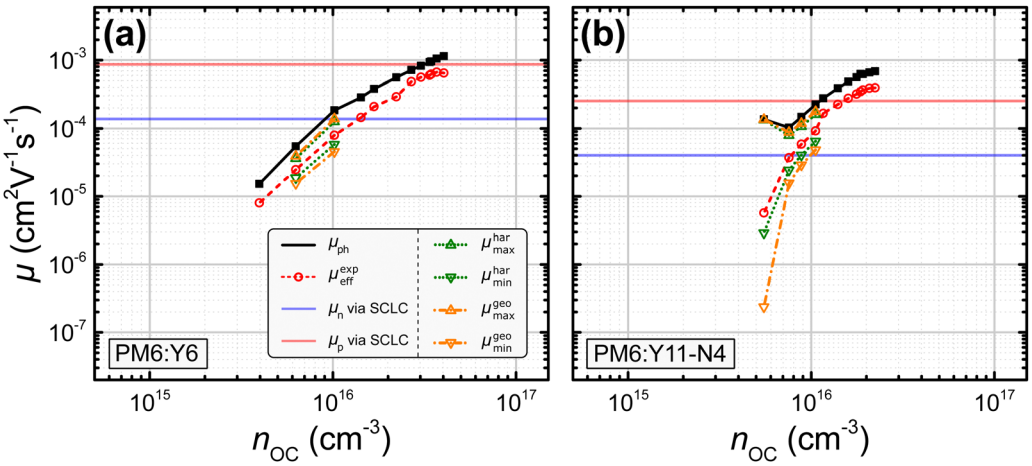

Fig. 3 Experimentally determined values for μ_{ph} (black squares; *cf.* eqn (4)) and μ_{eff}^{exp} (V_{OC}) (red circles; *cf.* eqn (3)) for a PM6:Y6 and a PM6:Y11-N4 organic solar cell. Calculation of the maximum and minimum mobilities determined *via* the harmonic and geometric approach (μ_{max}^{har}, μ_{min}^{har}: green dots, *cf.* eqn (8) and (9); μ_{max}^{geo}, μ_{min}^{geo}: orange dash-dots, *cf.* eqn (11) and (12)). The electron (μ_n: blue) and hole (μ_p: red) SCLC mobilities are shown as horizontal lines due to the unknown charge carrier density at which they were measured. Results for other investigated devices can be found in the ESI† (*cf.* Fig. S1).

The effective mobility under the open-circuit condition μ_{eff}^{exp} (V_{OC}) was obtained *via* linear interpolation of the experimentally determined values of μ_{eff}^{exp} at voltages close to open circuit, since according to eqn (3), μ_{eff}^{exp} (V_{OC}) is not directly accessible. To determine the photoconductance mobilities at open circuit by means of eqn (4), the real part of the device low-frequency admittance (also known as quasi-steady-state photoconductance G_{ph}) and the impedance-derived carrier density n were employed.[45,47] The results for PM6:Y6 (PDINO, L = 100 nm) and PM6:Y11-N4 in Fig. 3 serve well as a representation for the overall trends exhibited by the other blends (*cf.* Fig. S1 in the ESI†). The values of the photoconductance mobility μ_{ph} (black squares) and the interpolated values of μ_{eff}^{exp} (V_{OC}) (red circles), as well as other derived mobilities, are all visualized. Quite surprisingly, a relatively good agreement between the effective mobility at open circuit and half of the photoconductance mobility (μ_{eff}^{exp} (V_{OC}) $\approx 0.5\mu_{ph}$) was observed over a relatively wide range of charge carrier densities, which according to eqn (6) implies rather balanced electron and hole mobilities (*cf.* Fig. S1 of the ESI†). The only exception to this trend was PM6:N4, where a noticeable divergence at lower charge carrier densities is evident.

The values of μ_{max}^{har} and μ_{min}^{har} (green dots) as well as μ_{max}^{geo} and μ_{min}^{geo} (orange dash-dots) for the studied blends were calculated by inserting the experimentally determined μ_{ph} and μ_{eff}^{exp} either into eqn (8) and (9) or into eqn (11) and (12). The first set of equations is used, if the experimentally determined effective mobility μ_{eff}^{exp} is interpreted as the harmonic mean and the second set of equations is used, if μ_{eff}^{exp} is interpreted as the geometric mean. Interestingly, in case of the PM6:Y6 device, neither of these assumptions provided a continuous range of μ_{max} and μ_{min} values, as it was possible to obtain finite values only for a few data points. One explanation for this observation could be the relatively balanced charge carrier mobilities under the employed measurement conditions; then, even small deviations caused by measurement noise could push the ratio below the threshold of $\mu_{ph}/\mu_{eff} < 2$. Indeed, rather balanced mobilities have been reported for the PM6:Y6 blend.[54] In contrast, for the PM6:Y11-N4 solar cell it was possible to obtain finite values for both μ_{max} and μ_{min} at low to medium light intensities (*cf.* Fig. 3). In all cases where μ_{max} and μ_{min} could be obtained (*i.e.* $\mu_{ph}/\mu_{eff} \geq 2$), a greater imbalance between the individual mobilities was calculated when using μ_{eff}^{geo} in comparison to μ_{eff}^{har}. This observation is in agreement with Fig. 2(b), where a given ratio μ_{ph}/μ_{eff} would result in a more imbalanced ratio μ_p/μ_n, if μ_{eff}^{geo} was used rather than μ_{eff}^{har}. Interestingly, this line of reasoning also means that a hypothetical calculation of μ_{min} and μ_{max} based on μ_{eff}^{emp} (*cf.* Fig. 2) should yield even smaller ratios of μ_p/μ_n compared to the approach relying on μ_{eff}^{har}.

All studied blends can be divided into two categories exemplified by the two cells in Fig. 3. Specifically, the PM6:Y5, PM6:Y11, and various PM6:Y6 devices are comparable to the PM6:Y6 solar cell discussed in detail above, whereas the P3HT:$PC_{60}BM$, PM6:N4, and PPDT2FBT:Y6 solar cells are comparable to the PM6:Y11-N4 device (*cf.* Fig. S1 in the ESI†). The first category of blends only sporadically yielded finite values for μ_{max} and μ_{min}, while the latter category consistently yielded them, especially at lower charge carrier densities.

The individual mobilities of the studied blends determined *via* the SCLC method for single carrier diodes were added to Fig. 3 and Fig. S1 in the ESI† as a reference in the form of horizontal lines (μ_n: blue; μ_p: red). In general, SCLC mobilities are assumed to be obtained at charge carrier densities of $n \approx 10^{15}$–10^{16} cm^{-3}.[55] In case of the PM6:Y6 device shown in Fig. 3(a), the SCLC mobilities (μ_n = 1.3 × 10^{-4} cm^2 V^{-1} s^{-1}; μ_p = 8.4 × 10^{-4} cm^2 V^{-1} s^{-1}) are generally larger than the minimum and maximum mobilities determined *via* the harmonic and geometric approach at a charge carrier density of n = 10^{16} cm^{-3} (μ_{min}^{har} = 5.8 × 10^{-5} cm^2 V^{-1} s^{-1}; μ_{max}^{har} = 1.3 × 10^{-4} cm^2 V^{-1} s^{-1}; μ_{min}^{geo} = 4.6 × 10^{-5} cm^2 V^{-1} s^{-1}; μ_{max}^{geo} = 1.4 × 10^{-4} cm^2 V^{-1} s^{-1}). These deviations are not too surprising as only a few data points yielded finite values of μ_{min} and μ_{max}.

Table 2 Mobility ratios determined from the experimental methods in this study and reference mobilities for the studied blends. The reference mobilities were determined *via* the SCLC method

Blend	$\left(\frac{\mu_{max}}{\mu_{min}}\right)^{har}$	$\left(\frac{\mu_{max}}{\mu_{min}}\right)^{geo}$	μ_{min}^{ref} ($cm^2\ V^{-1}\ s^{-1}$)	μ_{max}^{ref} ($cm^2\ V^{-1}\ s^{-1}$)	$\left(\frac{\mu_{max}}{\mu_{min}}\right)^{ref}$	Ref.
P3HT:PC_{60}BM	1.94–34.94	2.57–339.61	2.0×10^{-4}	3.0×10^{-3}	15.0	56 and 57
PM6:Y11-N4	2.46–45.73	3.65–568.07	0.4×10^{-4}	2.5×10^{-4}	6.25	S20
PM6:Y5	1.59–2.69	1.93–4.17	3.3×10^{-4}	7.3×10^{-4}	2.1	S21
PPDT2FBT:Y6	1.41–2.68	1.63–4.15	1.5×10^{-4}	3.5×10^{-4}	2.3	S22
PM6:Y11	2.45	3.62	1.2×10^{-4}	1.6×10^{-4}	1.3	S23
PM6:N4	3.71–89.66	6.78–2098.70	0.1×10^{-4}	1.6×10^{-4}	16.0	58
PM6:Y6	1.68–3.52	2.09–6.27	1.3×10^{-4}	8.4×10^{-4}	6.5	58

However, in case of the PM6:Y11-N4 device shown in Fig. 3(b), the SCLC mobilities ($\mu_n = 4.0 \times 10^{-5}$ $cm^2\ V^{-1}\ s^{-1}$; $\mu_p = 2.5 \times 10^{-4}$ $cm^2\ V^{-1}\ s^{-1}$) more or less match the minimum and maximum mobilities determined *via* the harmonic and geometric approach at a charge carrier density of $n = 10^{16}$ cm^{-3} ($\mu_{min}^{har} = 6.5 \times 10^{-5}$ $cm^2\ V^{-1}\ s^{-1}$; $\mu_{max}^{har} = 1.6 \times 10^{-4}$ $cm^2\ V^{-1}\ s^{-1}$; $\mu_{min}^{geo} = 4.8 \times 10^{-5}$ $cm^2\ V^{-1}\ s^{-1}$; $\mu_{max}^{geo} = 1.8 \times 10^{-4}$ $cm^2\ V^{-1}\ s^{-1}$). Depending on the chosen charge carrier density, the reference SCLC mobilities of the other blend systems also show a reasonable agreement with the different determined values for μ_{min} and μ_{max} (*cf.* Fig. S1 in the ESI†), with the exception of the P3HT:PC_{60}BM solar cell, where the SCLC mobilities exceed the determined values for μ_{min} and μ_{max}. The values for μ_{min}, μ_{max}, and their ratios are listed in Table 2 for all investigated blend systems; the reference SCLC mobilities can be found in Section S24 of the ESI.† It turns out that the SCLC derived ratios for P3HT:PC_{60}BM, PM6:Y5, PPDT2FBT:Y6, PM6:Y11-N4, and PM6:N4 match well with the ratios determined *via* the harmonic and geometric approaches. In contrast, the SCLC derived ratios for PM6:Y6 and PM6:Y11 diverge from the ratios determined by the harmonic and geometric approach to a varying degree, which as mentioned previously might be caused by the few data points yielding finite values of μ_{min} and μ_{max}.

We note that mobilities reported in the literature for blends of organic semiconductors are generally determined *via* the SCLC technique, which relies on specifically fabricated single-carrier diodes that do not function as a solar cell and are typically operated at larger applied voltages. Thus, deviations between the SCLC derived parameters and the values determined in the scope of this study can also be caused by the difference in the applied conditions.[26]

Nonetheless, the observed agreement for most studied blend systems between the reference mobility ratios measured *via* SCLC and the ratios obtained *via* the effective mobility/photoconductance mobility analysis presented in this study has an important implication, validating these approaches relative to each other. It must be noted that the respective charge carrier densities, at which the mobilities are determined for both methods are quite close. Although the presented approach is unable to distinguish the sign of the faster/slower charge carriers, it allows both determining the values of μ_{min} and μ_{max} and checking if carrier mobilities are balanced (in which case $\mu_{eff}^{exp} = 0.5\ \mu_{ph}$ applies). As a result, this provides a new way to determine individual carrier mobilities in functioning solar cells at operating conditions, as well as rationalising the device performance due to a potentially present mobility imbalance.

4. Conclusions

In summary, we employed impedance spectroscopy measurements in a series of organic solar cells with different blend systems to determine both the effective and photoconductance mobilities (μ_{eff} and μ_{ph}). Furthermore, we demonstrated the possibility to determine the slower and faster mobilities (μ_{min} and μ_{max}) by solving systems of equations for μ_{eff} and μ_{ph}. For the studied solar cells, the values for μ_{min}, μ_{max}, and their ratio obtained by this approach match for the most part with the individual electron and hole mobilities, and their ratios, measured independently *via* the SCLC technique. The determination of finite values for μ_{min} and μ_{max} in a continuous range of light intensities was possible in the blends with higher mobility imbalance. In contrast, for the blends with rather balanced mobilities, finite values of μ_{min} and μ_{max} could not be obtained continuously. Importantly, this condition corresponds to the relationship between the effective and photoconductance mobilities: $\mu_{eff}^{exp} \approx 0.5\ \mu_{ph}$. This opens up an avenue to determine the effective mobility for such systems under open-circuit conditions without relying on interpolation or extrapolation.

Conflicts of interest

The authors declare that there is no conflict of interest regarding the publication of this article.

Acknowledgements

This work has been funded by the Alexander-von-Humboldt Stiftung [Sofja-Kovalewskaja-Award]. J. V. acknowledges funding by the Alexander-von-Humboldt Stiftung [Feodor-Lynen-Rückkehrstipendium] and by a Brückenstipendium of the University of Potsdam. H. Y. W. acknowledges the financial support from the National Research Foundation of Korea [2019R1A6A1A11044070].

References

1 G. Yu, J. Gao, J. C. Hummelen, F. Wudl and A. J. Heeger, Polymer photovoltaic cells: enhanced efficiencies via a network of internal donor-acceptor heterojunctions, *Science*, 1995, **270**, 1789–1791.
2 Y. J. Cheng, S. H. Yang and C. S. Hsu, Synthesis of conjugated polymers for organic solar cell applications, *Chem. Rev.*, 2009, **109**, 5868–5923.
3 G. Li, R. Zhu and Y. Yang, Polymer solar cells, *Nat. Photonics*, 2012, **6**, 153–161.
4 Y. Lin and X. Zhan, Oligomer molecules for efficient organic photovoltaics, *Acc. Chem. Res.*, 2016, **49**, 175–183.
5 L. Lu, T. Zheng, Q. Wu, A. M. Schneider, D. Zhao and L. Yu, Recent advances in bulk heterojunction polymer solar cells, *Chem. Rev.*, 2015, **115**, 12666–12731.
6 S. B. Darling and F. You, The case for organic photovoltaics, *RSC Adv.*, 2013, **3**, 17633–17648.
7 J. Guo and J. Min, A Cost Analysis of Fully Solution-Processed ITO-Free Organic Solar Modules, *Adv. Energy Mater.*, 2019, **9**, 1802521.
8 Y. Lin, Y. Firdaus, F. H. Isikgor, M. I. Nugraha, E. Yengel, G. T. Harrison, R. Hallani, A. El-Labban, H. Faber and C. Ma, *et al.*, Self-assembled monolayer enables hole transport layer-free organic solar cells with 18% efficiency and improved operational stability, *ACS Energy Lett.*, 2020, **5**, 2935–2944.
9 M. Zhang, L. Zhu, G. Zhou, T. Hao, C. Qiu, Z. Zhao, Q. Hu, B. W. Larson, H. Zhu and Z. Ma, *et al.*, Single-layered organic photovoltaics with double cascading charge transport pathways: 18% efficiencies, *Nat. Commun.*, 2021, **12**, 1–10.
10 Y. Cui, Y. Xu, H. Yao, P. Bi, L. Hong, J. Zhang, Y. Zu, T. Zhang, J. Qin and J. Ren, *et al.*, Single-Junction Organic Photovoltaic Cell with 19% Efficiency, *Adv. Mater.*, 2021, **33**, 2102420.
11 Y. Wei, Z. Chen, G. Lu, N. Yu, C. Li, J. Gao, X. Gu, X. Hao, G. Lu and Z. Tang, *et al.*, Binary organic solar cells breaking 19% via manipulating the vertical component distribution, *Adv. Mater.*, 2022, **34**, 2204718.
12 H. Yao and J. Hou, Recent Advances in Single-Junction Organic Solar Cells, *Angew. Chem.*, 2022, **134**, e202209021.
13 W. Gao, F. Qi, Z. Peng, F. R. Lin, K. Jiang, C. Zhong, W. Kaminsky, Z. Guan, C. S. Lee and T. J. Marks, *et al.*, Achieving 19% Power Conversion Efficiency in Planar-Mixed Heterojunction Organic Solar Cells Using a Pseudosymmetric Electron Acceptor, *Adv. Mater.*, 2022, **34**, 2202089.
14 Y. Lin, J. Wang, Z. G. Zhang, H. Bai, Y. Li, D. Zhu and X. Zhan, An electron acceptor challenging fullerenes for efficient polymer solar cells, *Adv. Mater.*, 2015, **27**, 1170–1174.
15 Y. Cui, H. Yao, L. Hong, T. Zhang, Y. Tang, B. Lin, K. Xian, B. Gao, C. An and P. Bi, *et al.*, Organic photovoltaic cell with 17% efficiency and superior processability, *Natl. Sci. Rev.*, 2020, **7**, 1239–1246.
16 A. Karki, J. Vollbrecht, A. J. Gillett, P. Selter, J. Lee, Z. Peng, N. Schopp, A. L. Dixon, M. Schrock and V. Nádaždy, *et al.*, Unifying charge generation, recombination, and extraction in low-offset non-fullerene acceptor organic solar cells, *Adv. Energy Mater.*, 2020, **10**, 2001203.
17 C. B. Nielsen, S. Holliday, H. Y. Chen, S. J. Cryer and I. McCulloch, Non-fullerene electron acceptors for use in organic solar cells, *Acc. Chem. Res.*, 2015, **48**, 2803–2812.
18 A. Kuzmich, D. Padula, H. Ma and A. Troisi, Trends in the electronic and geometric structure of non-fullerene based acceptors for organic solar cells, *Energy Environ. Sci.*, 2017, **10**, 395–401.
19 G. Zhang, J. Zhao, P. C. Chow, K. Jiang, J. Zhang, Z. Zhu, J. Zhang, F. Huang and H. Yan, Nonfullerene acceptor molecules for bulk heterojunction organic solar cells, *Chem. Rev.*, 2018, **118**, 3447–3507.
20 J. Hou, O. Inganäs, R. H. Friend and F. Gao, Organic solar cells based on non-fullerene acceptors, *Nat. Mater.*, 2018, **17**, 119–128.
21 Y. Xu, H. Yao, L. Ma, J. Wang and J. Hou, Efficient charge generation at low energy losses in organic solar cells: a key issues review, *Rep. Prog. Phys.*, 2020, **83**, 082601.
22 J. Lee, S. J. Ko, H. Lee, J. Huang, Z. Zhu, M. Seifrid, J. Vollbrecht, V. V. Brus, A. Karki and H. Wang, *et al.*, Side-chain engineering of nonfullerene acceptors for near-infrared organic photodetectors and photovoltaics, *ACS Energy Lett.*, 2019, **4**, 1401–1409.
23 R. Ma, T. Liu, Z. Luo, Q. Guo, Y. Xiao, Y. Chen, X. Li, S. Luo, X. Lu and M. Zhang, *et al.*, Improving open-circuit voltage by a chlorinated polymer donor endows binary organic solar cells efficiencies over 17%, *Sci. Chin. Chem.*, 2020, **63**, 325–330.
24 Q. Ma, Z. Jia, L. Meng, J. Zhang, H. Zhang, W. Huang, J. Yuan, F. Gao, Y. Wan and Z. Zhang, *et al.*, Promoting charge separation resulting in ternary organic solar cells efficiency over 17.5%, *Nano Energy*, 2020, **78**, 105272.
25 J. Yuan, Y. Zhang, L. Zhou, G. Zhang, H. L. Yip, T. K. Lau, X. Lu, C. Zhu, H. Peng and P. A. Johnson, *et al.*, Single-junction organic solar cell with over 15% efficiency using fused-ring acceptor with electron-deficient core, *Joule*, 2019, **3**, 1140–1151.
26 A. Karki, J. Vollbrecht, A. L. Dixon, N. Schopp, M. Schrock, G. M. Reddy and T. Q. Nguyen, Understanding the High Performance of over 15% Efficiency in Single-Junction Bulk Heterojunction Organic Solar Cells, *Adv. Mater.*, 2019, **31**, 1903868.
27 A. Karki, J. Vollbrecht, A. J. Gillett, S. S. Xiao, Y. Yang, Z. Peng, N. Schopp, A. L. Dixon, S. Yoon and M. Schrock, *et al.*, The role of bulk and interfacial morphology in charge generation, recombination, and extraction in non-fullerene acceptor organic solar cells, *Energy Environ. Sci.*, 2020, **13**, 3679–3692.
28 C. Yao, C. Peng, Y. Yang, L. Li, M. Bo and J. Wang, Larger VH (Hole Distribution Volume)/VM (Molecular Volume) Induced Higher Charge Mobility of Group IVA Element-Based Host Materials for Potentially Highly Efficient Blue OLEDs. The, *J. Phys. Chem. C*, 2018, **122**, 22273–22279.
29 C. Yao, C. Peng, Y. Yang, L. Li, M. Bo and J. Wang, Elucidating the key role of fluorine in improving the charge

mobility of electron acceptors for non-fullerene organic solar cells by multiscale simulations, *J. Mater. Chem. C*, 2018, **6**, 4912–4918.

30 C. Yao, Y. Yang, L. Li, M. Bo, C. Peng and J. Wang, Quadrotor-shaped non-fullerene electron acceptor materials with potential to enhance the photoelectric performance of organic solar cells, *J. Mater. Chem. A*, 2019, **7**, 18150–18157.

31 Y. Yang, C. Yao, L. Li, M. Bo, J. Zhang, C. Peng, Z. Huang and J. Wang, Non-fullerene electron acceptors constructed by four strong electron-withdrawing end groups: Potential to improve the photoelectric performance of organic solar cells by theoretical investigations, *Dyes Pigm.*, 2020, **181**, 108542.

32 C. Yao, Y. Yang, L. Li, M. Bo, J. Zhang, C. Peng, Z. Huang and J. Wang, Elucidating the key role of the cyano (- C≡ N) group to construct environmentally friendly fused-ring electron acceptors, *J. Phys. Chem. C*, 2020, **124**, 23059–23068.

33 Y. Yang, C. Yao, L. Li, M. Bo, M. He and J. Wang, Isomerization of two-dimensional non-fullerene electron acceptor materials for developing high-performance organic solar cells, *J. Mater. Chem. C*, 2022, **10**, 11286–11295.

34 N. S. Sariciftci, Polymeric photovoltaic materials, *Curr. Opin. Solid State Mater. Sci.*, 1999, **4**, 373–378.

35 M. P. Hughes, K. D. Rosenthal, N. A. Ran, M. Seifrid, G. C. Bazan and T. Q. Nguyen, Determining the dielectric constants of organic photovoltaic materials using impedance spectroscopy, *Adv. Funct. Mater.*, 2018, **28**, 1801542.

36 J. Vollbrecht, J. Lee, S. J. Ko, V. V. Brus, A. Karki, W. Le, M. Seifrid, M. J. Ford, K. Cho and G. C. Bazan, *et al.*, Design of narrow bandgap non-fullerene acceptors for photovoltaic applications and investigation of non-geminate recombination dynamics, *J. Mater. Chem. C*, 2020, **8**, 15175–15182.

37 S. Shoaee, M. Stolterfoht and D. Neher, The Role of Mobility on Charge Generation, Recombination, and Extraction in Polymer-Based Solar Cells, *Adv. Energy Mater.*, 2018, **8**, 1703355.

38 M. C. Heiber, T. Okubo, S. J. Ko, B. R. Luginbuhl, N. A. Ran, M. Wang, H. Wang, M. A. Uddin, H. Y. Woo and G. C. Bazan, *et al.*, Measuring the competition between bimolecular charge recombination and charge transport in organic solar cells under operating conditions, *Energy Environ. Sci.*, 2018, **11**, 3019–3032.

39 J. Vollbrecht, V. V. Brus, S. J. Ko, J. Lee, A. Karki, D. X. Cao, K. Cho, G. C. Bazan and T. Q. Nguyen, Quantifying the nongeminate recombination dynamics in nonfullerene bulk heterojunction organic solar cells, *Adv. Energy Mater.*, 2019, **9**, 1901438.

40 C. Shuttle, A. Maurano, R. Hamilton, B. O'regan, J. C. de Mello and J. Durrant, Charge extraction analysis of charge carrier densities in a polythiophene/fullerene solar cell: Analysis of the origin of the device dark current, *Appl. Phys. Lett.*, 2008, **93**, 183501.

41 J. W. Ryan and E. Palomares, Photo-Induced Charge Carrier Recombination Kinetics in Small Molecule Organic Solar Cells and the Influence of Film Nanomorphology, *Adv. Energy Mater.*, 2017, **7**, 1601509.

42 K. Nakano, Y. Chen and K. Tajima, Quantifying charge carrier density in organic solar cells by differential charging techniques, *AIP Adv.*, 2019, **9**, 125205.

43 C. M. Proctor, C. Kim, D. Neher and T. Q. Nguyen, Nongeminate recombination and charge transport limitations in diketopyrrolopyrrole-based solution-processed small molecule solar cells, *Adv. Funct. Mater.*, 2013, **23**, 3584–3594.

44 E. Von Hauff, Impedance spectroscopy for emerging photovoltaics, *J. Phys. Chem. C*, 2019, **123**, 11329–11346.

45 J. Vollbrecht and V. V. Brus, On charge carrier density in organic solar cells obtained via capacitance spectroscopy, *Adv. Electron. Mater.*, 2020, **6**, 2000517.

46 J. Vollbrecht, N. Tokmoldin, B. Sun, V. V. Brus, S. Shoaee and D. Neher, Determination of the charge carrier density in organic solar cells: A tutorial, *J. Appl. Phys.*, 2022, **131**, 221101.

47 N. Tokmoldin, J. Vollbrecht, S. M. Hosseini, B. Sun, L. Perdigón-Toro, H. Y. Woo, Y. Zou, D. Neher and S. Shoaee, Explaining the Fill-Factor and Photocurrent Losses of Nonfullerene Acceptor- Based Solar Cells by Probing the Long-Range Charge Carrier Diffusion and Drift Lengths, *Adv. Energy Mater.*, 2021, **11**, 2100804.

48 A. Wagenpfahl, Mobility dependent recombination models for organic solar cells, *J. Phys.: Condens. Matter*, 2017, **29**, 373001.

49 S. Albrecht, J. R. Tumbleston, S. Janietz, I. Dumsch, S. Allard, U. Scherf, H. Ade and D. Neher, Quantifying charge extraction in organic solar cells: the case of fluorinated PCPDTBT. The, *J. Phys. Chem. Lett.*, 2014, **5**, 1131–1138.

50 S. Schiefer, B. Zimmermann and U. Würfel, Determination of the intrinsic and the injection dependent charge carrier density in organic solar cells using the Suns-VOC method, *J. Appl. Phys.*, 2014, **115**, 044506.

51 D. Neher, J. Kniepert, A. Elimelech and L. Koster, A new figure of merit for organic solar cells with transport-limited photocurrents, *Sci. Rep.*, 2016, **6**, 1–9.

52 A. Armin, J. Subbiah, M. Stolterfoht, S. Shoaee, Z. Xiao, S. Lu, D. J. Jones and P. Meredith, Reduced Recombination in High Efficiency Molecular Nematic Liquid Crystalline: Fullerene Solar Cells, *Adv. Energy Mater.*, 2016, **6**, 1600939.

53 P. Kaienburg, U. Rau and T. Kirchartz, Extracting Information about the Electronic Quality of Organic Solar-Cell Absorbers from Fill Factor and Thickness, *Phys. Rev. Appl.*, 2016, **6**, 024001.

54 Q. An, X. Ma, J. Gao and F. Zhang, Solvent additive-free ternary polymer solar cells with 16.27% efficiency, *Sci. Bull.*, 2019, **64**, 504–506.

55 C. Tanase, E. J. Meijer, P. W. M. Blom and D. M. de Leeuw, Unification of the Hole Transport in Polymeric Field-Effect Transistors and Light-Emitting Diodes, *Phys. Rev. Lett.*, 2003, **91**(21), 216601.

56 V. D. Mihailetchi, H. Xie, B. Boer, L. A. de, Koster and P. W. Blom, Charge transport and photocurrent generation

in poly (3-hexylthiophene): methanofullerene bulk-heterojunction solar cells, *Adv. Funct. Mater.*, 2006, **16**, 699–708.
57 F. Laquai, D. Andrienko, R. Mauer and P. W. Blom, Charge carrier transport and photogeneration in P3HT:PCBM photovoltaic blends, *Macromol. Rapid Commun.*, 2015, **36**, 1001–1025.
58 L. Perdigón-Toro, L. Q. Phuong, F. Eller, G. Freychet, E. Saglamkaya, J. I. Khan, Q. Wei, S. Zeiske, D. Kroh and S. Wedler, *et al.*, Understanding the Role of Order in Y-Series Non-Fullerene Solar Cells to Realize High Open-Circuit Voltages, *Adv. Energy Mater.*, 2022, **12**, 2103422.